Response Surface Method Optimization of Uniform and Axially Segmented Duct Acoustics Liners

L. Lafronza,* A. McAlpine,† A. J. Keane,‡ and R. J. Astley§
University of Southampton, Highfield, England SO17 1BJ, United Kingdom

An extensive duct acoustics propagation study is presented that has been conducted to assess the design of a liner for an aeroengine inlet duct. The aim is to predict how different liner configurations, at various flight conditions, affect the attenuation of sound in an inlet. Two different noise source models are used: single mode and multimode. These represent the two principal fan noise sources: tonal and broadband noise. The two noise source models are then combined to predict the overall attenuation. An optimization procedure based on a response surface model is presented, to investigate a uniform and an axially segmented acoustic liner. The objective function used in the optimization is based on an approximate calculation of the perceived noise level. The aim is to utilize an axially segmented liner to increase, compared to a uniform liner, the overall sound attenuation that is predicted. The main feature that emerges is that it is possible to increase the attenuation with an axially segmented liner only when a limited number of propagating modes are present.

Nomenclature

A_{mn}	=	modal pressure amplitude
B	=	number of fan blades
B_{mn}	=	modal velocity amplitude
b	=	duct radius, m
c_0	=	speed of sound, $\mathrm{m \cdot s^{-1}}$
$\mathcal{F}$	=	shaft rotation frequency, Hz
f	=	frequency, Hz
$f_{1/3}()$	=	center third-octave band frequency
h	=	liner face-sheet cavity depth, m
I_x	=	modal acoustic intensity in the axial direction, $\mathrm{W \cdot m^{-2}}$
i	=	$\sqrt{-1}$
J_m	=	Bessel function of the first kind of order m
j, t	=	integer index
k	=	free space wave number, $\mathrm{rad \cdot m^{-1}}$
$k_{x_{mn}}$	=	radial wave number, mode (m, n), $\mathrm{rad \cdot m^{-1}}$
$k_{x_{mn}}$	=	axial wave number, mode (m, n), $\mathrm{rad \cdot m^{-1}}$
L	=	duct length, m
L_{hw}	=	length of hard-walled duct section, m
L_{sw}	=	length of lined duct section, m
l_1	=	length of the first segment of the axially segmented liner, m
M_x	=	axial Mach number
m	=	azimuthal mode order
N_d	=	number of design of experiments initial design points
N_L	=	number of axial acoustic liner segments
N_r	=	number of scattered modes used in mode matching
n	=	radial mode order
p_0	=	static pressure, Pa
p'	=	acoustic pressure, Pa
R	=	reduced liner resistance
r, θ, x	=	cylindrical polar coordinates
u_0	=	uniform mean flow velocity vector, $\mathrm{m \cdot s^{-1}}$
u'	=	acoustic particle velocity vector, $\mathrm{m \cdot s^{-1}}$
W_{in}	=	incoming sound power at the fan plane, W
W_{out}	=	outgoing sound power at the exit plane, W
W_{mn}	=	sound power of mode (m, n), W
X_c	=	reduced cavity reactance
X_m	=	reduced face-sheet mass reactance
Z	=	reduced liner impedance
β_{mn}	=	cutoff ratio
ρ_0	=	mean flow density, $\mathrm{kg \cdot m^{-3}}$
$\rho_0 c_0$	=	characteristic impedance, $\mathrm{Pa \cdot s \cdot m^{-1}}$
ω	=	angular frequency, $2\pi f$, $\mathrm{rad \cdot s^{-1}}$

I. Introduction

WITH the growth of many cities, more people now live near an airport. Therefore, to meet new noise-level criteria a lot of effort has been invested by researchers in aeroacoustics to reduce noise emissions from aircraft engines. In a typical turbofan engine, fan and exhaust noises are among the major components of the noise signature of an aircraft. A typical frequency spectrum of a turbofan aircraft engine will contain tonal[1] and broadband noise components.[2-4] Because of the different nature of the two noise components, it is possible to study them separately.

Starting from the fundamental work by Tyler and Sofrin,[1] fan tonal noise, whether generated by a rotor-alone pressure field or rotor–stator interaction, can be modeled by rotating pressure patterns called spinning modes. Fan tonal noise has been a prevalent feature of aircraft noise since the entry into service in the 1970s of high-bypass-ratio aircraft engines.[5] At subsonic tip speeds, the dominant tones are due to rotor–stator interactions. These tones are defined as modes spinning at the harmonics of the engine blade passing frequency.[1] At supersonic fan speeds, the dominant fan tones are due to the rotor-alone pressure field. At this condition, aeroengines are known to generate an acoustic signature that contains energy spread over a wide range of harmonics of the engine shaft rotation frequency.[1-6] This results in a large number of tones present in the noise spectrum.

When a broad frequency spectrum is studied, sound levels at subsonic fan speeds are often dominated by the continuous background noise, also called broadband noise.[7] Modeling of broadband noise has always been a challenging problem because of the complicated nature of the noise-generation mechanism. However, prediction of broadband noise levels is required to assist strategies for reducing overall levels of fan noise. In the text that follows, we take a simple equal power per mode distribution for this noise source and model only the propagation of the resulting sound field, rather than its generation.

The acoustic propagation model can be formulated by using the linearized Euler equations (LEE) or a convected form of the second-order wave equation in pressure or velocity potential. The LEE formulation is commonly solved by using high-order finite difference models[8] or finite element models based on the discontinuous Galerkin method (see Refs. 9 and 10). The wave equation formulation is usually solved by conventional finite and infinite element models, or by more unconventional schemes, such as the Green function discretization (see Ref. 11). In this study, a semi-analytic method based on acoustic modes propagating in a circular-section cylindrical duct is used, with the acoustic pressure field modeled as a sum of Fourier–Bessel modes (see Eversman[12]). Based on this representation of the acoustic pressure, models for tonal and broadband noise are proposed. In fact, it is not entirely correct to define the models as tonal and broadband. It is more accurate to refer to them as single-mode and multimode models. They are designed, however, to characterize tonal and broadband noise in a duct.

The broadband noise source is modeled by inclusion of all of the propagating (cuton) modes, over a wide frequency range. The main assumption is that at each frequency the acoustic power is divided equally among all of the propagating modes and all of the modes are uncorrelated.[13]

The nature of the tonal noise source depends on the engine power condition, that is, whether the fan tip speed is subsonic or supersonic. At subsonic fan tip speeds, modes that represent rotor–stator interaction tones, at the harmonics of blade passing frequency, are present. Here it is assumed these modes will be contained within the multimode broadband components. At supersonic fan tip speeds, tonal noise is modeled by tones at the harmonics of the shaft rotation frequency. In this case, the propagating circumferential mode order is equal to the harmonic order of the shaft rotation frequency, and close to the fan, only the first radial mode order is considered to be significant.

The aim of this paper is to assemble a procedure to predict an optimum liner configuration that maximizes the noise reduction (referenced to a hard-wall condition). The use of a nonuniform axial impedance distribution offers the potential to increase sound absorption, without introducing scattering into different azimuthal mode orders.

Following the early papers by Rice[14–16] on acoustic liner optimization, more recent papers have attempted more advanced liner optimization studies. For example, the use of a multimode source to represent broadband noise has been reported in Refs. 17–19. Also of interest is the effect of circumferentially nonuniform impedance distributions, such as those reported in Refs. 20–23. In these previous studies, only a small number of propagating modes have been considered, with an optimization performed only over a narrow range of frequencies.

In this paper, modes are used to model both types of source: tonal and broadband noise. The inlet duct and mean flow are modeled by a circular-section cylindrical duct that contains a constant uniform mean-flow (Fig. 1). The duct is segmented into a hard-walled inlet section, a number of acoustically treated sections, and a hard-walled exit section.
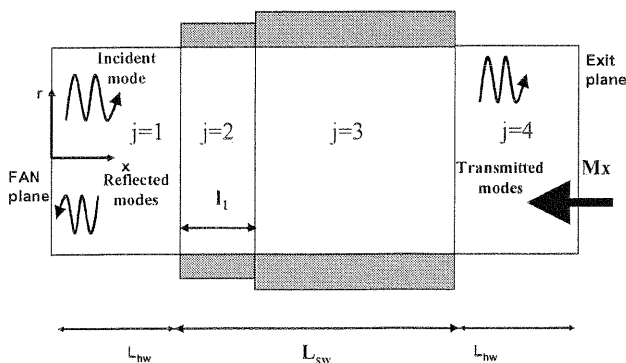

Fig. 1   Mode-matching method applied to the axially segmented liner.

A series of optimization studies have been conducted to predict how different liner configurations, at various flight conditions, affect the attenuation of sound. Our aim is to predict whether there is any benefit in using a piecewise axially varying impedance, referred to as an axially segmented liner, instead of a uniform liner that has a constant impedance. One aspect of having an axially varying impedance is the potential it offers for increasing sound attenuation because of modal scattering. The scattering due to an impedance change at the duct wall is modeled by using mode matching, in which continuity of pressure and axial velocity is applied across the cross section of the duct; see, for example, Cummings[24] and Lansing and Zorumski.[25]

In the optimization process, the variables used to define the locally reacting liner are the face-sheet resistance R and the cavity depth h. At each frequency, the transmission of all of the propagating modes is calculated separately. Then the sound power in each third-octave-frequency band is reduced to a single value associated with the third-octave center frequency. Finally, an approximate weighted integration is conducted over these center frequencies to calculate the objective function (or cost function). In this case an approximate perceived noise level (PNL) algorithm is used.[26]

In the case of a uniform liner, a two-dimensional optimization problem is solved because the liner is defined by two design variables, namely, R and h. When an axially segmented liner is examined, a larger number of variables is involved and an appropriate search engine must be used. The aim is to yield a good design by using a reduced number of new design points to map the search space. In such circumstances, response surface modeling is a useful optimization tool. The optimization procedure used here is based on the use of design of experiments (DOE) methods,[27,28] to build an ensemble of sample points, and kriging to build a response surface model (RSM).[29] This is a surrogate model of the real function that will be searched instead of the real problem. The parallel capability of the DOE method, and the use of a surrogate model, strongly reduces the computational time. The result is a reduction of the effort expended in searching in areas of poor design, giving a reliable optimum by using only a limited number of function evaluations. To verify the method presented here, the uniform liner optimization problems have been solved using this procedure and also a contour map has been built in the (R, h) plane.

All of the optimization techniques used within this paper are included in the optimization software package Options.[30] The software is a design exploration package assembled over the years by Keane. It includes a particularly powerful and varied suite of optimizers covering a wide range of methods that users are able to tune and assemble for their own specific problems.

II. Acoustics Model

Modeling sound propagation in a real turbofan inlet duct is a challenging task. However, to demonstrate the optimization process, it is sufficient to consider only a relatively simple model for the inlet duct. In the following analysis, the inlet is modeled as a duct with uniform circular cross section, containing a uniform mean flow with Mach number $M_x < 1$.

The acoustic propagation model is based on the linearized set of equations governing the isentropic motion of a nonviscous, non-heat-conducting perfect gas.[12] The linearized acoustic equations are obtained by considering small perturbations to a mean state ρ_0, p_0, and u_0. It is assumed that an unspecified noise source introduces harmonic disturbances with time dependence $e^{i\omega t}$. The resulting acoustic fluctuations in the duct can then be written as $p = p'e^{i\omega t}$, where p' now satisfies the convected Helmholtz equation. In cylindrical polar coordinates (r, θ, x) it is well known that on separating the variables r, θ, and x the acoustic pressure can be expressed as a Fourier–Bessel modal sum, with modes defined as

$$p'_{mn} = A_{mn} J_m\left(k_{r_{mn}}r\right) \exp\left[i\left(-m\theta - k_{x_{mn}}x\right)\right] \tag{1}$$

The radial wave numbers $k_{r_{mn}}$ are determined by application of an appropriate boundary condition and then solving the resulting eigenvalue equation.[12] It is found that for an acoustically lined duct, $k_{r_{mn}}$ is

a complex number, and for a hard-walled duct, $k_{r_{mn}}$ is real. To speed up the calculation in the hard-walled duct, the eigenvalue solution is loaded from an external table.[31] In the lined duct, to avoid missing any modes, a standard fourth-order Runge–Kutta method, followed by a Newton–Raphson search, is implemented (see Ref. 32), starting with the solution for the hard-walled duct.[33] At this point, the solution is checked, as if there is a double eigenvalue, then the mode-matching procedure (Sec. II.E) cannot be used. The liner optimization procedure requires a large number of modes to be calculated for different values of f, M_x, and Z. In general, for most of the simulations there is no double eigenvalue. However, because of the large number of simulations required for the optimization process, there were instances when two eigenvalues with very similar values were found. Then, there is less accuracy using the mode-matching procedure (because of ill conditioning), but fortunately this problem was quite rare.

Then $k_{x_{mn}}$ is given by

$$k_{x_{mn}} = \left[k / \left(1 - M_x^2\right)\right]\left[-M_x \pm \sqrt{1 - (1/\beta_{mn})^2}\right] \quad (2)$$

with

$$\beta_{mn} = k / k_{r_{mn}} \sqrt{1 - M_x^2} \quad (3)$$

In a hard-walled duct, the cutoff ratio defines which mode (m, n) is propagating $(\beta_{mn} > 1)$ and which is decaying $(\beta_{mn} \leq 1)$. Following the paper by Rice,[16] a spinning mode may be defined as highly propagating (large β_{mn}) when the acoustic wave motion is mainly in the axial direction. While near cutoff $(\beta_{mn} \rightarrow 1)$, the wave motion is mainly transverse or circumferential. Then, it follows that the axial wave number [Eq. (2)] associated with mode (m, n) is real for $\beta_{mn} > 1$ and complex for $\beta_{mn} < 1$. It can be easily shown that the so called cutoff modes $(\beta_{mn} < 1)$ do not transmit any acoustic power because they are decaying modes.

In a lined duct, all of the modes have complex axial wave number because the radial wave number is complex. Therefore, when a liner is present, modes are neither cuton nor cutoff, but any mode of order (m, n) has an axial decay rate given by $\exp(\text{Im}\{k_{x_{m.n}}\}x)$.

To assess the sound power transmitted by the modal pressure field, it is necessary to take into account the mean flow. In Ref. 34, the definition of acoustic intensity for a hard-walled duct, valid for any flow that is isentropic and irrotational, is given by

$$I_{x_{mn}} = \left(|p'_{mn}|^2 / 2\rho_0 c_0\right)\left\{\left(1 + M_x^2\right)\text{Re}\left[k_{x_{mn}} / \left(k - M_x k_{x_{mn}}\right)\right]\right.$$

$$\left. + M_x\left[1 + \left|k_{x_{mn}} / \left(k - M_x k_{x_{mn}}\right)\right|^2\right]\right\} \quad (4)$$

The sound power of a single mode W_{mn} is found by integrating $I_{x_{mn}}$ over the cross section of the duct. Using the orthogonal property of the Bessel function the integration yields

$$W_{mn} = (\pi / 2\rho_0 c_0)\left[b^2 - \left(m^2 / k_{r_{mn}}^2\right)\right]\left|J_m\left(k_{r_{mn}} b\right)\right|^2 |A_{mn}|^2$$

$$\times \left\{\left(1 + M_x^2\right)\text{Re}\left[k_{x_{mn}} / \left(k - M_x k_{x_{mn}}\right)\right]\right.$$

$$\left. + M_x\left[1 + \left|k_{x_{mn}} / \left(k - M_x k_{x_{mn}}\right)\right|^2\right]\right\} \quad (5)$$

Therefore, with an expression for the modal sound power at the fan and exit plane (Fig. 1) obtained, the modal sound power transmission loss $\Delta_{\text{PWL}_{mn}}$ across the duct, for the incoming mode order (m, n), is defined as

$$\Delta_{\text{PWL}_{mn}} = 10 \log_{10}\left(W_{\text{in}_{mn}} \middle/ \sum_j W_{\text{out}_{mj}}\right) \quad (6)$$

In Eq. (6), $W_{\text{in}_{mn}}$ is the power associated with the single incoming mode of order (m, n) at the fan plane, and $W_{\text{out}_{mj}}$ is the power of the propagating (scattered) mode of order (m, j) at the exit plane. The summation is performed over all of the propagating modes.

The sound power spectrum, for the lined duct, is found by subtracting the values of $\Delta_{\text{PWL}_{mn}}$ from the sound power spectrum for the hard-walled duct. Realistic noise spectra for a hard-walled inlet duct,

at different flight conditions, have been provided by Rolls–Royce, plc., for use in this optimization study. Once the sound power spectrum is calculated at each design configuration, the objective function used is the PNL, which is evaluated using a frequency weighted integration.

A. PNL

The PNL is a quantity of relevant interest to engine manufacturers, and so this is used as the objective function. It is well known that the basic element for noise certification criteria is the noise evaluation measure known as effective PNL (EPNL), which is a single-number evaluator of the subjective effects of aircraft noise on human beings, over a given time interval. EPNL consists of instantaneous PNL, that is, PNL(t), corrected for spectral irregularities and for duration. In this study, the instantaneous PNL is used as the objective function in the optimization procedure. The calculation procedure for this quantity is well explained in the advisory circular of the U.S. Department of Transportation, Federal Aviation Administration.[26] The instantaneous PNL is a function of the instantaneous one-third octave band sound power levels. This spectrum is converted into perceived noise and then combined to produce the total perceived noise. Finally, the total perceived noise is converted to perceived noise decibels.

B. Single-Mode Model

It is well known that the fan tones that are generated by an aero-engine are highly dependent on the engine power or fan speed. Two components of the tonal noise can be defined depending on the generation mechanism. These are rotor-alone tones and rotor–stator interaction tones. Here only the rotor-alone tones, present when the fan tip speed is supersonic, are taken in consideration. This is because the rotor–stator interaction tones are less significant, compared to the broadband noise, when a large bandwidth spectrum is used.

Typically, in a turbofan inlet duct the dominant fan tones are the harmonics of blade passing frequency. In fact, for a perfect fan, the only tones that are generated will be engine orders (EO), which are multiples of the number of fan blades, B. In practice, however, because of blade-to-blade differences, variations in stagger angles, and other imperfections, a full set of engine order tones is typically present, that is, $EO = m = 1, 2, 3, \ldots$, with peaks when m is a multiple of the blade number B. This produces a frequency spectrum for the rotor-alone pressure field comprising tones with frequency $m\mathcal{F}$, $m = 1, 2, 3, \ldots$.

For this kind of tonal noise, the supersonic flow at the fan tip extends over a small region close to the duct wall. Here, it is assumed that most of the propagating energy is associated with the first radial mode order $(n = 1)$, even when at higher frequencies more than one radial mode order will be cuton. Therefore, a first approximation of the rotor-alone pressure field close to the fan, following the Fourier–Bessel modal representation, is to include only the first radial mode order for all of the EO taken in consideration.

At a given shaft rotation frequency $\mathcal{F}$, all of the tones that are harmonics of $\mathcal{F}$, that is, the EO tones, are included. Each tone is modeled as a single mode with radial order $n = 1$. Once the noise level is calculated at each EO, the spectrum is reduced to the standard third-octave-band frequency spectrum, from which the objective function is evaluated. In this study, the frequency spectrum in consideration is limited to the first 18 one-third octave bands. This means that the highest frequency used is $f_{1/3}(18) = 7500$ Hz.

Now, the objective function used here is a function of the transmission loss spectrum at the center third-octave-band frequencies, whereas the EO spectrum depends on the engine speed, which is different for the different flight conditions tested. Therefore, to reduce the EO spectrum to a third-octave spectrum (containing the first 18 third-octave bands), an appropriate number of EO have to be included in the analysis. In the examples in this paper, a minimum of 59 EO were required to calculate up to $f_{1/3}(18)$.

C. Multimode Model

When a broadband noise model is used, an important issue is the definition of an energy spectrum distribution. The type of source

model will affect the optimum liner design.[13] Here the noise propagation is modeled by a multimode source, for which the sound power at each frequency is fixed, and is spread equally over all of the propagating modes. The number of propagating modes depend on the frequency and also the Mach number of the mean flow.

It is also assumed that all of the modes are uncorrelated. This means that the propagation of each propagating mode is calculated individually, and then the transmitted energy can be summed to determine the transmission loss at each frequency. As a consequence, because the definition of a phase for each of the modes is merely a random decision, due to the complicated noise-generation mechanism for this sound source, all of the incoming modes are assumed to have a phase equal to zero. This assumption is supported by a statistical study, see the Appendix.

The multimode model requires that, at each frequency, all of the possible cuton modes are evaluated individually, whereas the single-mode model only requires one mode to be calculated at each frequency. Therefore, the multimode model requires significantly more computational time. (In practice hundreds of modes may be calculated to use with the multimode model.) This also means that at each frequency the total amount of power in and out is

$$W_{\text{in/out}} = \sum W_{mn\,\text{in/out}}$$

where the summation is over all of the incoming (in) and propagating scattered (out) modes.

In the multimode study, the discrete frequencies needed to build the power spectrum are taken to be the center third-octave frequencies. Also, as before, the frequency spectrum is limited to the first 18 third-octave bands.

D. Liner Model

Typical acoustic liners used in turbofan ducts consist of a perforated face-sheet bonded to a honeycomb core. Because the aim here is to find the liner design that maximizes the attenuation of the sound, a model to predict the acoustic impedance is required. A number of models have been developed to estimate the acoustic impedance of locally reacting liners. The most common acoustic liners are single-cavity liners (SDOF—single degree of freedom) but double cavity liners (two degree of freedom) are also used. The type of liner determines the specific acoustic impedance Z at the duct wall. In this work, a SDOF liner model has been used. The reduced specific acoustic impedance is defined as

$$Z = R + i(X_m + X_c) = R + i[km_r - \cot(k\,h)] \qquad (7)$$

where Z is normalized by the characteristic impedance $\rho_0 c_0$. The face-sheet mass reactance $X_m = km_r$ is assumed to be proportional to the frequency. The quantity m_r is usually assumed to depend on the thickness and porosity of the face sheet; for further details see Motsinger and Kraft.[35] A value of $m_r = 0.005$ m is used in all of the calculations presented here. Also, note that the resistance R is assumed to be independent of frequency.

To predict the most absorbent liner, the face-sheet resistance R and the cavity depth h are used as liner design variables in the optimization procedure.

E. Mode-Matching Theory

In an axisymmetric duct containing a finite length of acoustic lining, scattering will occur where there is a change in the acoustic impedance at the duct wall. There is no scattering between azimuthal modes but only among different radial modes because the impedance is uniform in the circumferential direction. An appropriate scheme

is needed to relate the acoustic pressure and particle velocity on either side of an impedance discontinuity. To take account of modal scattering, a mode-matching formulation is used.[24,25] This approach may be viewed as being rather simplistic because an alternative approach would be to use a finite element method, which could model more complex variations in the liner's impedance. However, the aim is to demonstrate that a liner optimization that includes modeling of tonal and broadband noise sources can be carried out in a practical timescale using modern computational resources. In the first instance, a simple acoustic propagation code, mode matching, is used. In future work, it is planned to replace the use of the mode-matching code with a more sophisticated approach such as the finite element method.

The acoustic pressure at each axial position is written as a superposition of Fourier–Bessel modes,

$$p'(r, \theta, x) = \sum_{m,n} \left[A_{mn}^+ J_m\left(k_{r_{mn}}^+ r\right) e^{-ik_{x_{mn}}^+ x} \right.$$
$$\left. + A_{mn}^- J_m\left(k_{r_{mn}}^- r\right) e^{-ik_{x_{mn}}^- x} \right] e^{im\theta} \qquad (8)$$

where the superscripts $\pm$ are associated with waves propagating in the positive or negative x direction, respectively. Note that the radial and axial wave numbers take different values in the different regions of the duct (hard and lined wall). The corresponding axial particle velocity is given by

$$u_x'(r, \theta, x) = \sum_{m,n} \left[B_{mn}^+ J_m\left(k_{r_{mn}}^+ r\right) e^{-ik_{x_{mn}}^+ x} \right.$$
$$\left. + B_{mn}^- J_m\left(k_{r_{mn}}^- r\right) e^{-ik_{x_{mn}}^- x} \right] e^{im\theta} \qquad (9)$$

(using the same notation as earlier) where, from the acoustic momentum equation,

$$B^{\pm} = \left[k_x^{\pm} / \rho_0 \left(\omega - k_x^{\pm} u_0 \right) \right] A^{\pm} = d^{\pm} A^{\pm} \qquad (10)$$

For a fixed azimuthal mode order m, at the interface between two different regions in the duct, continuity of pressure and axial particle velocity can be expressed in weak form as

$$\int_{r=0}^{r=b} r J_m\left(k_{r_{mn}} r\right) \left\{ \begin{bmatrix} p'^{(j)} \\ u_x'^{(j)} \end{bmatrix} - \begin{bmatrix} p'^{(j+1)} \\ u_x'^{(j+1)} \end{bmatrix} \right\} dr = 0 \qquad (11)$$

where the superscript $j = 1, 2, \ldots, N_L + 1$ specifies two adjacent areas with different impedance values. In this paper, two adjacent liner segments are considered, as shown Fig. 1, but the method works for as many liner segments as required. For each radial mode order, that is $n = 1, 2, \ldots, N_r$, this yields a system of $(N_L + 1) \cdot N_r$ unknowns $(A_{mn}^{(j)\pm}, B_{mn}^{(j)\pm})$, with $2N_r$ equations at each interface. The number of radial mode orders that is used is equal to the number of possible cuton modes plus 10 cutoff radial modes. An acoustic surface wave mode may be included in this set of modes, but the hydrodynamic surface wave instability (Rienstra[36]) is not included. Now when Eq. (11) is applied at each location where a liner impedance discontinuity is present, and Eq. (10) is used, the system to solve can be written as

$$V \begin{bmatrix} A_{mn}^{(j)+} \\ A_{mn}^{(j+1)-} \end{bmatrix} = U \begin{bmatrix} A_{mn}^{(j+1)+} \\ A_{mn}^{(j)-} \end{bmatrix} \qquad (12)$$

The vectors $A^{\pm}$ are of length N_r, and V and U are $(2N_r, 2N_r)$ square matrices, composed of four (N_r, N_r) matrices, given by

$$V = \left[\begin{array}{c|c} v_{it}^{(j+1)+} & v_{it}^{(j)-} \\ \hline d_{it}^{(j+1)+} v_{it}^{(j+1)+} & d_{it}^{(j)-} v_{it}^{(j+1)-} \end{array} \right] \qquad (13)$$

$$U = \left[\begin{array}{c|c} v_{it}^{(j)+} \exp\left\{-k_{x_{mi}}^{(j)+} [x_j - x_{(j-1)}]\right\} & v_{it}^{(j+1)-} \\ \hline d_{it}^{(j)+} v_{it}^{(j)+} & d_{it}^{(j+1)-} v_{it}^{(j+1)-} \exp\left\{-k_{x_{mi}}^{(j+1)-} [x_j - x_{(j+1)}]\right\} \end{array} \right] \qquad (14)$$

where $d_{it}^{(j)\pm}$ is given in Eq. (10) and $v_{it}^{(j)\pm}$ is

$$v_{it}^{(j)\pm} = \int_{r=0}^{r=b} r J_m \left(k_{r_{mi}} r \right) J_m \left(k_{r_{mt}}^{(j)\pm} r \right) dr \qquad (15)$$

Here $k_{r_{mi}}$ denotes a solution of $J'_m (k_{r_{mi}} b) = 0$, and $k_{r_{mt}}^{(j)\pm}$ is the corresponding radial wave number for the mode of order (m, t) in the sector (j) for positive or negative propagating modes. To avoid problems associated with ill conditioning, an iterative procedure[24] is used to solve Eqs. (12) at each location where there is a change in the impedance. In this case, the duct is assumed to be anechoically terminated, and so there are no reflected modes in the outlet section, that is, $A_{mn}^{(j)-} = 0$, $j = N_L + 2$. The amplitudes of the incoming modes are assumed to be known, e.g., equal energy per mode in the multi-mode analysis, and the transmission of each mode, specified by (m, n), is calculated independently.

The mode-matching code utilized for this liner optimization study has been benchmarked against the finite element method. Details of this benchmark will be published by McAlpine et al.[37] and so are not repeated here.

III. Optimization Methods

An objective of the current study is to examine the potential increase in noise attenuation for an axially segmented liner compared to a uniform liner. Two different liner optimization studies have been conducted. First, a uniform liner is studied using only two design variables to specify the acoustic impedance, namely, the face-sheet resistance R and the liner cavity depth h. In this case, a complete search of the (R, h) plane is possible, mapping a discrete number of possible configurations. When the number of variables increases, a more efficient optimization procedure must be used. Several techniques are available. However, all of these methods are time consuming when the objective function is expensive to calculate. This makes the number of simulations (objective function evaluations) used to generate a suitable design an important issue.[38]

A relatively new optimization method is to build a surrogate model and to search this model instead.[19,39–41] This is an RSM. The basic RSM process involves selecting a limited number of points at which the numerical simulations are run, normally using formal DOE methods.[27] When these simulations have been performed, usually in parallel, a surrogate for the objective and constraint (if there are any) functions is built, by fitting a response surface through or near the data, as explained by Jones[29] and Keane.[30] Design optimization is then carried out on this surface to locate potential combinations of the design variables that appear to minimize or maximize the cost function. These may then be fed back into the full code and can be used to update the model. The whole process is repeated until some form of convergence is achieved, or an acceptable design has been obtained. There are a number of variations and refinements that may be applied to the basic RSM approach. Here the general approach used takes a Latin hypercube modified DOE (LPτDOE) method to form the sequence of initial DOE points and a kriging method to build the RSM.[29,38] (The acronym comes from the variables L, P, and τ used in Sobol's paper.[42]) Most DOE methods seek to sample the entire design space by building an array of possible designs with relatively even, but not constant, spacing between the points. A particular advantage of the LPτDOE approach is that not only does it give good coverage for engineering design purposes, but it also allows additional points to be added to a design without the need to reposition existing points.[42] Then, if the initial build of the RSM is found to be inadequate, a new set of points can be inserted without invalidating the statistical character of the experiments.

After the array of data points is built, from which a surface can be constructed, a decision has to be made whether to regress (as opposed to interpolate) the data. In this case, the RSM model is built using a kriging approach with regularization. This method allows the user to control the amount of regression (smoother) as well as provides a theoretically sound basis for judging the degree of curvature needed to model the user's data adequately. Kriging also provides measures of probable errors in the model being built that can be used when assessing where to place any further points.[38] To

Table 1 Optimization procedure validation

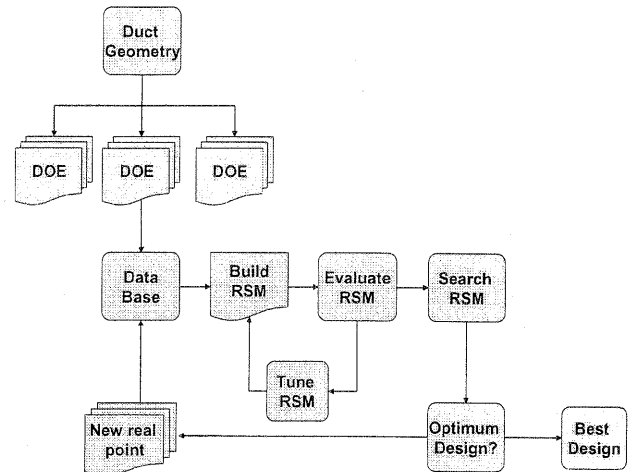| Design space	Contour map	$N_d = 20$ First update	$N_d = 20$ Second update	$N_d = 40$
R	10	9.6	10	10
Depth cm	1.1	1.1	1.1	1.1
PNL	6.67	6.62	6.67	6.67

Fig. 2 Optimization process.

control this error, a two-stage search of the likelihood function has been carried out, using in series a genetic algorithm[43] (GA) and a dynamic hill climbing method[44] to tune the hyper parameters that define the kriging RSM. Finally, a similar two-stage search has to be carried out on the RSM itself to find a new set of points that will be added to the database of sample points used to build the RSM. This process is shown in Fig. 2.

To validate the procedure proposed, all of the optimization studies reported here for the uniform liner configuration have been analyzed using a contour map search and the meta-modeling technique. When the contour map search is used, the two-dimensional space (R, h) is simply mapped with a fine grid of equispaced points. The optimum value of (R, h) is then easily located. The same problem is then solved using initially 20 and then 40 DOE points, followed by a single update search on the RSM built through the initial set of points. The definition of sample points needed to first represent the metamodel is crucial when a surrogate model is used. A general rule says that 10 points per dimension search should be enough to build the initial RSM. In all of the optimizations presented here, more than 10 points per dimension are used. This means that the updating process will start from a more accurate surface and, in theory, should converge faster.

A single-design point, running on a personal computer, (Intel Pentium 4, 2.52 GHz), takes on average approximately 10 min for the single-mode (SM) model and 45 min for the multimode (MM) model. There is a large reduction in runtime achieved when an RSM methodology is used compared with a contour map search. An even greater benefit (using RSM) will be achieved for higher dimensional optimization problems. In Table 1, an example of the results (for the uniform liner) are shown for the three optimizations used: contour map, RSM with 20 DoE points and RSM with 40 DoE points. When 40 DoE points are used the exact optimum is predicted within a single update, whereas when 20 points are used at least 2 update processes are needed. This example is for the SM model at the sideline fan speed, see Sec. IV.

IV. Results

As already discussed, the aim of this paper is to demonstrate that it is possible to assemble a complete liner design optimization procedure, for different acoustic propagation models and different flight conditions.

Table 2 Fan operating conditions

Operating condition	Sideline	Cutback	Approach
M_x	−0.5	−0.44	−0.27
rpm	9687	8158	5608
$\mathcal{F}$	161.4	136	63.5

Table 3 Test cases

	Flight condition/fan speed			
Noise source	Sideline	Cutback	Approach	AFS
SM	√	√	Cutoff	√
MM	√	√	√	√
SM + MM	√	√	√	√

In this study, two liner configurations are considered: a uniform liner and an axially segmented liner. A set of optimum liner configurations at three different fan speeds, typical of the sideline, cutback, and approach flight conditions, are predicted for the two acoustic models. Table 2 shows the Mach numbers and revolutions per minute used in this study. This example is based on a one-third-scale inlet test rig, at realistic flight conditions. A second set of optimizations have been performed searching for an optimum liner suitable for all of the fan speeds (AFS). The optimum liner is regarded as the "best" compromise between the different optimum configurations at each fan speed. For each fan speed, three different source models are used. These are representative of the rotor-alone pressure field (SM), the broadband noise (MM), and the two sources combined together (SM + MM). Table 3 shows all of the cases that have been examined.

The optimization study is based on an idealized inlet geometry, represented as a circular cross-section straight duct. In Fig. 1, the duct is shown. The duct has radius $b = 0.43$ m, and the overall length of lining is $L_{sw} = 0.344$ m. The liner design variables, the reduced resistance R, and liner cavity depth h are searched over the range $R = [1, 10]$ and $h = [0.2, 2]$ cm. Note that the liner depth is equivalent to a range [0.6, 6] cm at full-scale engine size. Note that the typical depth of a turbofan inlet liner is about 3 cm. The range of resistance values used for the optimization study is larger than one might expect to use in a real aircraft inlet. The typical reduced resistance of a turbofan inlet liner is usually not greater than four. It is found that for higher engine powers, a high resistance increases the attenuation of the rotor-alone modes. However, such a high-resistance value will not be suitable at other flight conditions, and so an alternative optimization is presented in the cases where the optimum resistance value exceeds the value of four. A second set of optimizations is then run, for which the maximum value of the resistance is constrained to be $R \le 4$. This is a more realistic value for the type of lining used in a turbofan inlet duct.

The objective function used in all the cases is the PNL, which is a function of the sound power levels at the third-octave band center frequencies. In this study the first 18 third-octave bands are used. When the MM source model is used, the spectrum is defined by a set of discrete frequencies equal to the third-octave center frequencies. Whereas when the SM source model is optimized, the first 59 engine orders are used. These frequencies are each multiples of the shaft rotation frequency. Then, this spectrum is reduced to a third-octave-frequency spectrum, which is used as input for the objective function. The criteria used to select the right number of engine orders to include in the analysis are based on the need to reduce this spectrum to the first 18 third-octave-bands, that is, $f_{1/3}\{18\} = 7500$ Hz. Therefore, from Table 2, the highest frequencies used for the SM model are sideline $f = 59\mathcal{F} = 9528.5$ Hz and cutback $f = 59\mathcal{F} = 8024$ Hz. For the two source models (SM + MM) combined together, the spectrum for the objective function is given by a unitary weighted summation of the sound power spectrum obtained from the two models, at the third-octave center frequencies.

The three noise source models are used to predict the optimum liner configuration at each of the fan speeds listed in Table 2. Also,

an optimum that can be considered a compromise between all of the different fan speeds is found. Therefore, an appropriate decibel-weighted average of the PNL values at each fan speed is required for the objective function, which is used to predict the optimum for AFS. A weighted average is used, although in this case only a unitary weighting is applied to each fan speed. A more sophisticated weighting could be used if desired.

The strategy used to find the best configuration is the same for each optimization problem. First, an initial base of N_d design points are generated with an LPτDOE distribution and evaluated in parallel; here $N_d = 200$ for the axial liner (five variables), and $N_d = 40$ for the uniform liner (two variables). For the uniform liner case, the most straightforward and accurate approach is to span the design space and to build a complete map of the two-dimensional space. When the optimization technique proposed here is used, the search time for the two-dimensional optimization problem is reduced by a factor of three, compared to a contour map method built with a 11 by 11 grid for a two-dimensional search. Consequently, the method is even more efficient when the search is performed over a design space with dimension greater than two. In fact, depending on the number of processors used during the DOE points generation and updating process, the optimizer is able to locate an optimum in a time given by

$(N_d +$ number of update)

× model running time/number of parallel processes

The average runtimes (per design point) on a personal computer are 10 and 45 min for the SM and MM models, respectively. Usually 10 parallel processes are used. Then the number of update points are 25 for the axial liner, and 2 for the uniform liner. Therefore, the typical runtime to predict an optimum uniform liner configuration is about 1 h for the SM model and about 8 h for the MM model. Whereas to predict an optimum axially segmented liner configuration takes about 15 h for the SM model and about 96 h (4 days) for the MM model. When the two basic models are combined, the resulting runtime is given by the sum of the different models' individual runtimes. All of the uniform liner optimum design points shown in the following results have been predicted using both search methodologies: the response surface method and the contour map.

For all of the cases in Table 3, results are presented in the form of tables and supported by contour plots. In all the results shown, the liner depth is in centimeters, the relative liner length l_1 is given as a percentage of the total liner length L_{sw}, and the objective function is presented as an increment Δ_{PNL} with respect to the PNL value without a liner, that is, the noise level with a hard-walled inlet duct.

A. Uniform Liner

In this section, the optimization results for the circular duct with a uniform liner are presented. The optimum values located in the design space are listed in Tables 4–6, and contour plots of the RSM objective function in the (R, h) space are shown in Figs. 3–5.

Table 4 Uniform liner: optimum resistance and liner depth for the three fan speeds, at sideline, cutback, and approach

Design space	Sideline			Cutback			Approach
	MM	SM	SM + MM	MM	SM	SM + MM	MM
$R(\le 10)$	5.4	10	7.3	3.7	3.5	3.7	2.6
h, cm	1.63	1.1	1.52	1.48	1.14	1.46	1.34
Δ_{PNL}	1.78	6.67	4.30	1.62	19.78	5.00	1.43

Table 5 Uniform liner: optimum resistance and liner depth at sideline, with resistance constrained to $R \le 4$

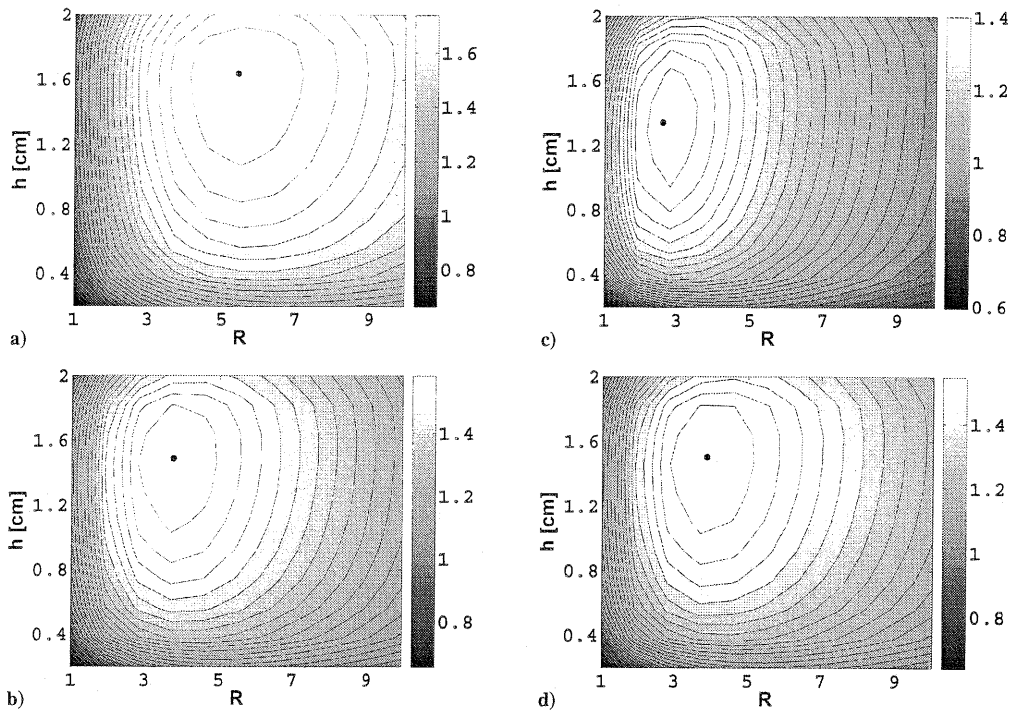| Design space	MM	SM	SM + MM
$R(\le 4)$	4	4	4
h, cm	1.63	1.46	1.5
Δ_{PNL}	1.74	5.00	3.80

Fig. 3   Uniform liner, contour maps of Δ_{PNL} for MM model with dots at optimum locations at a) sideline, b) cutback, c) approach, and d) AFS.
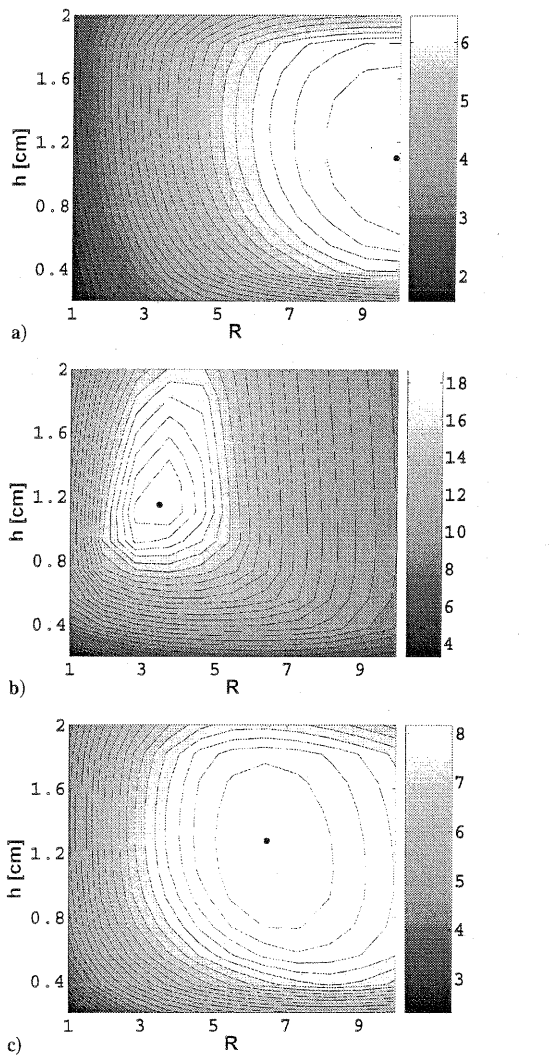

Fig. 4   Uniform liner, contour maps of Δ_{PNL} with dots at optimum locations for SM model at a) sideline, b) cutback and c) AFS.
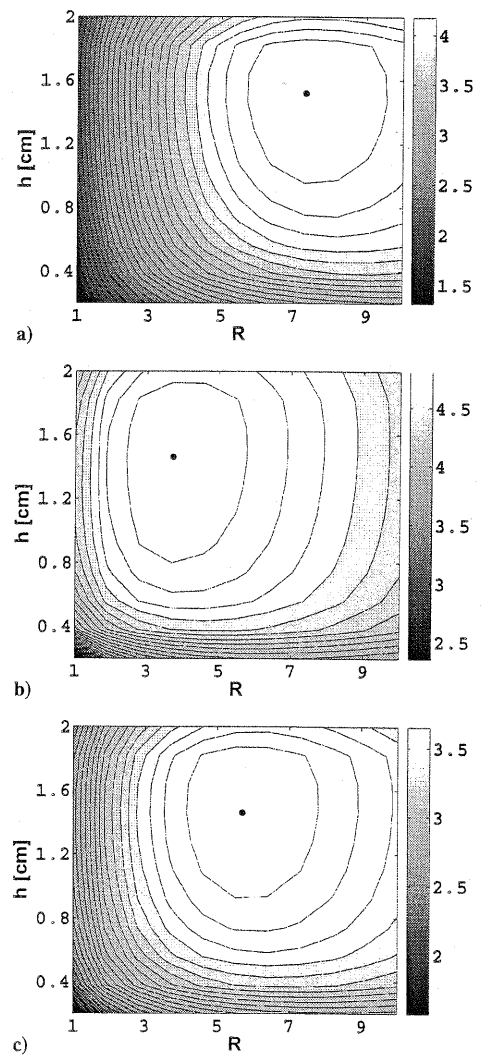
Fig. 5   Uniform liner, contour maps of Δ_{PNL} with dots at optimum locations for MM + SM model at a) sideline, b) cutback and c) AFS.

The optimum values of the design variables R and h and the relative attenuation Δ_{PNL} are listed in Table 4, for the sideline, cutback, and approach conditions. Figures 3, 4, and 5 show contour plots for the optimum values in the (R, h) plane, for the MM, SM, and the combined source models, respectively. At the approach condition, the rotor-alone pressure field is cutoff, and only the MM source is considered.

For the highest fan speed, that is, sideline, the optimum liner resistance is typically greater than 5, and for the SM source, the optimum resistance is 10. However, at cutback and approach, the optimum value of the resistance is less than 4. Typical resistances for real engine liners are seldom greater than 4, and so the optimum value at sideline is rather unrealistic. Therefore, a second set of

Table 6   Uniform liner: optimum resistance and liner depth for AFS and Δ_{PNL} at each fan speed

Noise source	R	h, cm	Sideline	Cutback	Approach	AFS
			$R \leq 10$			
MM	3.9	1.50	1.7	1.6	1.4	1.58
SM	6.5	1.27	6.2	13.7	——	8.42
SM + MM	5.7	1.46	4.2	4.8	1.2	3.74
			$R \leq 4$			
SM	4	1.28	5.0	19.2	——	7.78
SM + MM	4	1.46	3.8	5.0	1.4	3.65

optimizations have been performed, with the liner resistance constrained to be $R \leq 4$. The results are presented in Table 5 for the sideline case. As expected, the optimum is $R = 4$. If the predicted values of Δ_{PNL} with $R \leq 4$ are compared to the corresponding values in Table 4 with $R \leq 10$, a significant reduction in attenuation is predicted when $R \leq 4$. The difference is about 1.7 dB for the SM and about 0.5 dB for the SM + MM model, but a negligible reduction is found for the MM model.

Tables 4 and 5 give optimal liner parameters obtained independently for each engine condition. The optimal parameters when the three engine conditions are combined (AFS) is shown in Table 6 and Figs. 3d, 4c, and 5c. Here the objective function is defined by an appropriate decibel-weighted average of the values of PNL at each fan speed. Table 6 lists not only the overall attenuation Δ_{PNL}, but also the relative values of Δ_{PNL} at each fan speed. When the optimum resistance exceeds the value of four, another optimization is run using $R \leq 4$. As before, the optimum resistance tends to the upper value of the permitted resistance range. However, the reduction in attenuation achieved when the resistance is constrained to be $R \leq 4$ is less than 0.5 dB, compared with allowing $R \leq 10$.

In all cases, the optimum liner depth is about the same irrespective of whether the resistance is constrained. This confirms that there is a limited range of cavity depth that produces a good performance.

The MM model optimum for the combined flight engine conditions (AFS), as shown in Fig. 3d, is similar to cutback (Fig. 3b), probably because the optimum is a compromise between the sideline
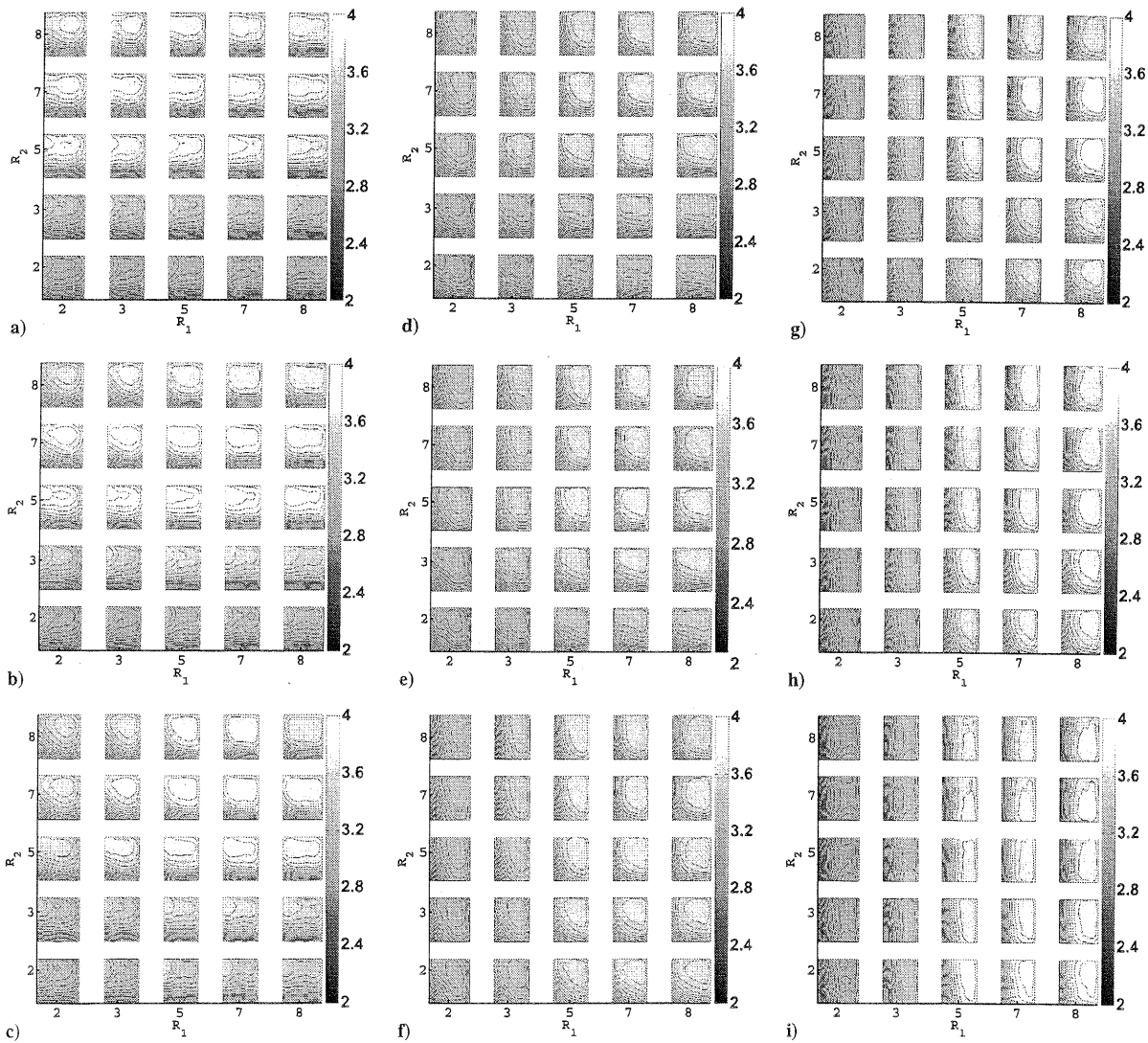

Fig. 6   5D HAT plot for axially segmented liner, for various l_1/L_{sw} a) 12, b) 27, c) 35, d) 50, e) 58, f) 66, g) 74, h) 82, and i) 98%.

and the approach condition. Whereas for the SM model, Fig. 4c, the dominant factor is the sideline fan speed. Finally, an optimum for the combined source models (SM + MM) at sideline, cutback, and AFS is shown in Fig. 5c.

From the data presented, some conclusions are made regarding the behavior of the three source models: SM, MM, and SM + MM. It is found that the attenuation slightly increases with fan speed when an MM model is used, but decreases for the SM model. It is also seen that higher resistances are more effective at the highest fan speed. The optimum resistance decreases as the fan speed is reduced. Conversely, the liner depth depends on the type of model used. In fact, for the SM model, a shallow liner at high fan speeds and a thicker liner at other lower speeds is predicted. The opposite requirement is found for the MM model. Finally, when the two models are searched together, the optimum prediction is a compromise between the individual sources, with a tendency to be close to the case with the lowest attenuation.

B.   Axially Segmented Liner

The second set of optimization results are for an axially segmented liner. There are five design variables, the liner resistances R_1 and

R_2, cavity depths h_1 and h_2, and the first liner relative length l_1/L_{sw}, where L_{sw} is fixed. Because it is impractical to sample the full space, and to verify the results in the same way as the two-dimensional problem, the recurrence of the optimum for four or more searches on the RSM is used as a convergence criterion.

A way to visualize the solution in the design space is the use of a five-dimensional hierarchical axes technique (HAT) as shown in Fig. 6. Figure 6 contains most of the information needed to analyze the axially segmented liner optimization. To better read the five-dimensional HAT results, a single contour plot is first examined. The horizontal and vertical axes are h_1 and h_2 (not shown), and the Δ_{PNL} contours are for a fixed value of the resistances R_1 and R_2 and the relative liner length l_1/L_{sw}. Next examine one of the nine ensembles of contour plots. Each of these plots is for a fixed value of l_1/L_{sw}. The outer axes are the values of the liner resistance R_1 and R_2. Then, at a fixed value of l_1/L_{sw}, and for each combination of discrete values of R_1 and R_2, a single contour plot can be seen as a function of h_1 and h_2. Finally, when Fig. 6 is viewed overall, the objective function over the design space at discrete values of resistance and length is shown. Note that all of the plots are on the same color scale. Because of limited space, only the HAT plot for
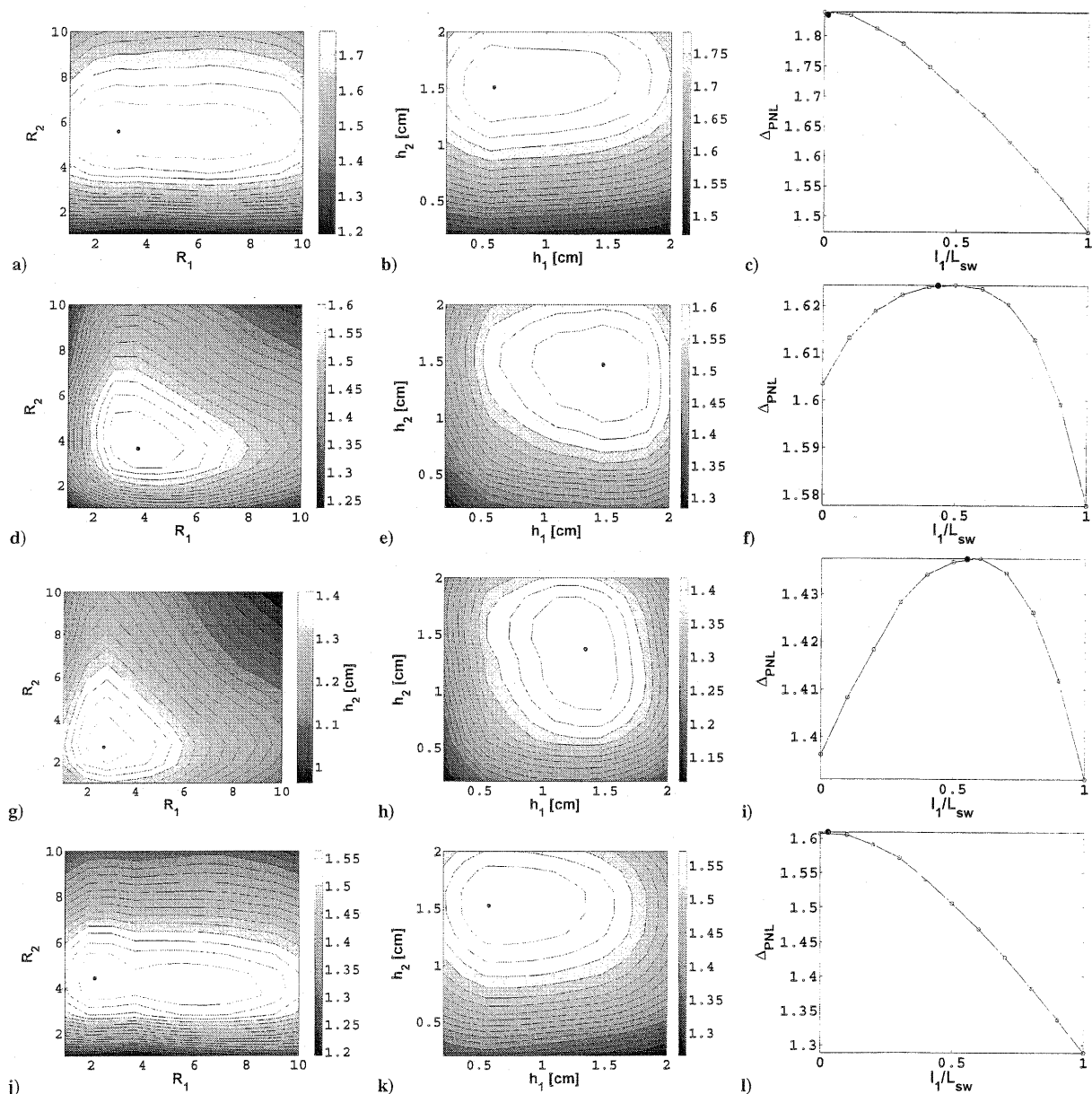

Fig. 7   Axially segmented liner, MM model, Δ_{PNL} variation with respect to different combinations of R_1 and R_2 a, d, g, and j), h_1 and h_2 b, e, h, and k), and l_1/L_{sw} c, f, i, and l), at fan speeds a–c) sideline, d–f) cutback, g–i) approach, and j–l) AFS. Other variables fixed at optimum condition.
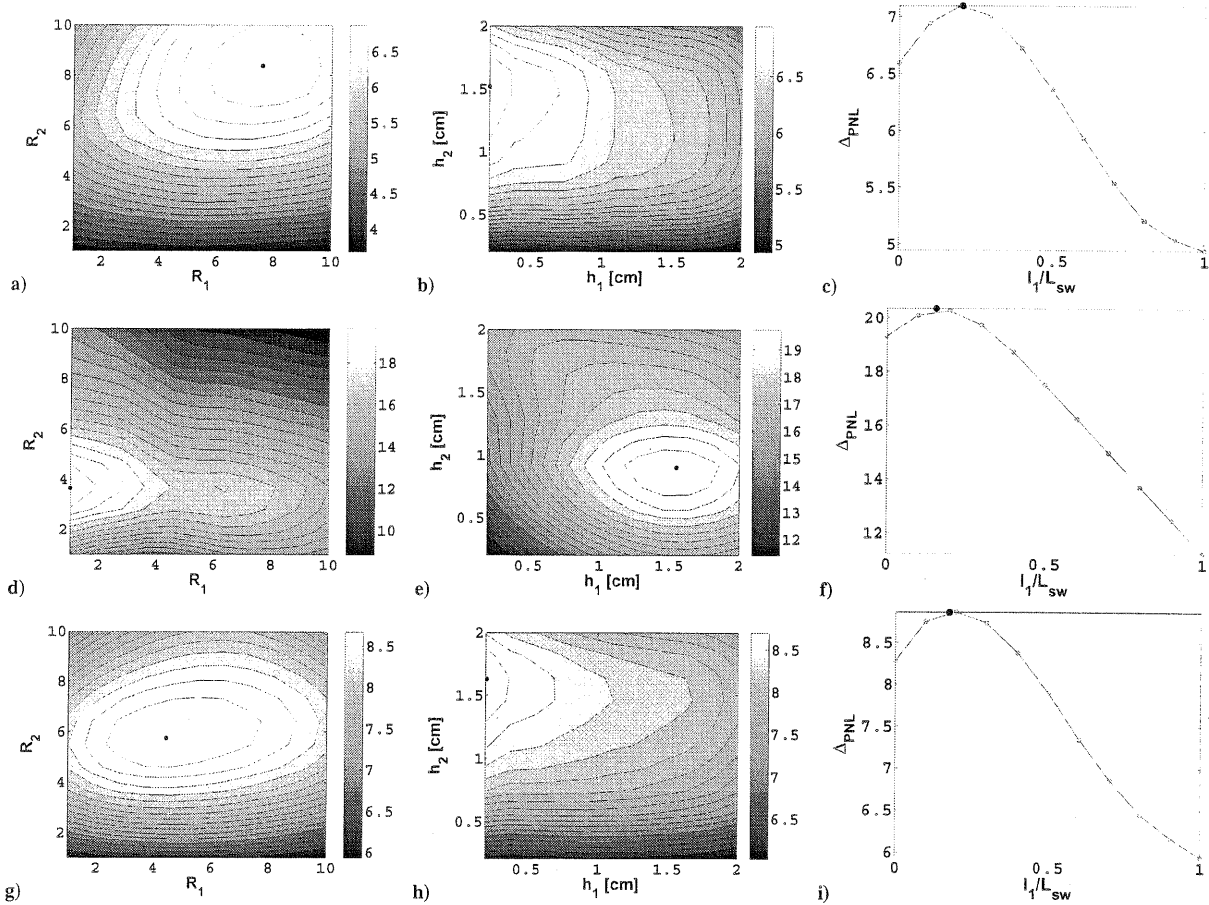
Fig. 8 Axially segmented liner, SM model Δ_{PNL} variation with respect to different combinations of a, d, and g) R_1 and R_2, b, e, and h) h_1 and h_2, and c, f, and i) l_1/L_{sw}, at fan speeds, a–c) sideline, d–f) cutback, and g–i) AFS.

one optimization is shown. This is for the AFS problem. Although this visualization technique is useful to show how the metaobjective function covers the design space, it is not guaranteed that the region where the absolute optimum is located, if there is one, is included. In fact, in Fig. 6, the color scale used is upper limited by the optimum value of Δ_{PNL}, which is found. Nonetheless, this kind of multidimensional visualization technique is extremely useful to represent the metaobjective function shape in the design space. In fact, if the optimizer fails, this information will be used to restrict the search to a region where a better performance is predicted.

Along with the HAT plot, Figs. 7–9 show the Δ_{PNL} variation with R_1 and R_2, h_1 and h_2, and l_1/L_{sw} for the optimum values listed in Tables 7 and 8. Figures 7–9 clearly show the location of the optimum for each case. In Table 9, the predicted values of Δ_{PNL} is shown for the different fan speeds and source models based on the optimum for the AFS problem. The attenuation increases with the engine power for the MM model and decreases for the SM model.

An interesting feature is that sometimes the optimum for the axially segmented liner is a uniform liner. This is particularly true for the MM model. In fact, for each of the flight conditions we have examined, the optimum liner configuration for this source model converges to the uniform liner. These results suggest that the use of an axially segmented liner to attenuate broadband noise will not produce any real benefit. It seems that any potential benefit due to modal scattering is negated by the high number of propagating modes.

The reason that the optimum that is predicted is believed to be unique is due to the nature of the problem in consideration. In fact a requirement of the proposed RSM modeling method is that the surface that is built is by definition a continuous function, so any spikes in the real function tend to be smoothed by the RSM. In this case, the objective function is definitely a smooth and continuous

Table 7   Axially segmented liner: optimum resistance, liner depth, and liner length for sideline, cutback and approach

Noise source	R_1	R_2	h_1, cm	h_2, cm	l_1/L_{sw}, %	Δ_{PNL}
			Sideline, $R_1 \le 10$ and $R_2 \le 10$			
MM	2.9	5.6	0.59	1.51	1.5	1.82
SM	7.6	8.4	0.20	1.52	21	7.10
SM + MM	4.6	6.7	0.22	1.65	10.5	4.40
			Cutback, $R_1 \le 10$ and $R_2 \le 10$			
MM	3.7	3.6	1.47	1.47	43.5	1.62
SM	1.0	3.6	1.55	0.90	16	20.3
SM + MM	2.3	4.0	0.63	1.50	1.5	5.00
			Approach, $R_1 \le 10$ and $R_2 \le 10$			
MM	2.7	2.7	1.34	1.37	55	1.43
			Sideline, $R_1 < 4$ and $R_2 < 4$			
MM	4	3.2	1.7	0.5	100	1.74
SM	4	4	0.2	1.6	24	6.00
SM + MM	4	4	0.2	1.6	22	4.20

function. Therefore, because the updating process is performed in parallel, searching in different areas of the design space at the same time, it is found that after a sufficient number of updates, usually about 25, the optimizer converges to a unique optimum.

When the SM source model is used, an increase in attenuation of about 0.5 dB is predicted at the different fan speeds for the axially segmented liner compared to the uniform liner. When both source models are combined, the maximum attenuation, predicted at either sideline or cutback, is similar for both the axially segmented or uniform liners. However, when all of the fan speeds are combined together, an increase in attenuation of about 0.43 dB is predicted with the axially segmented liner.
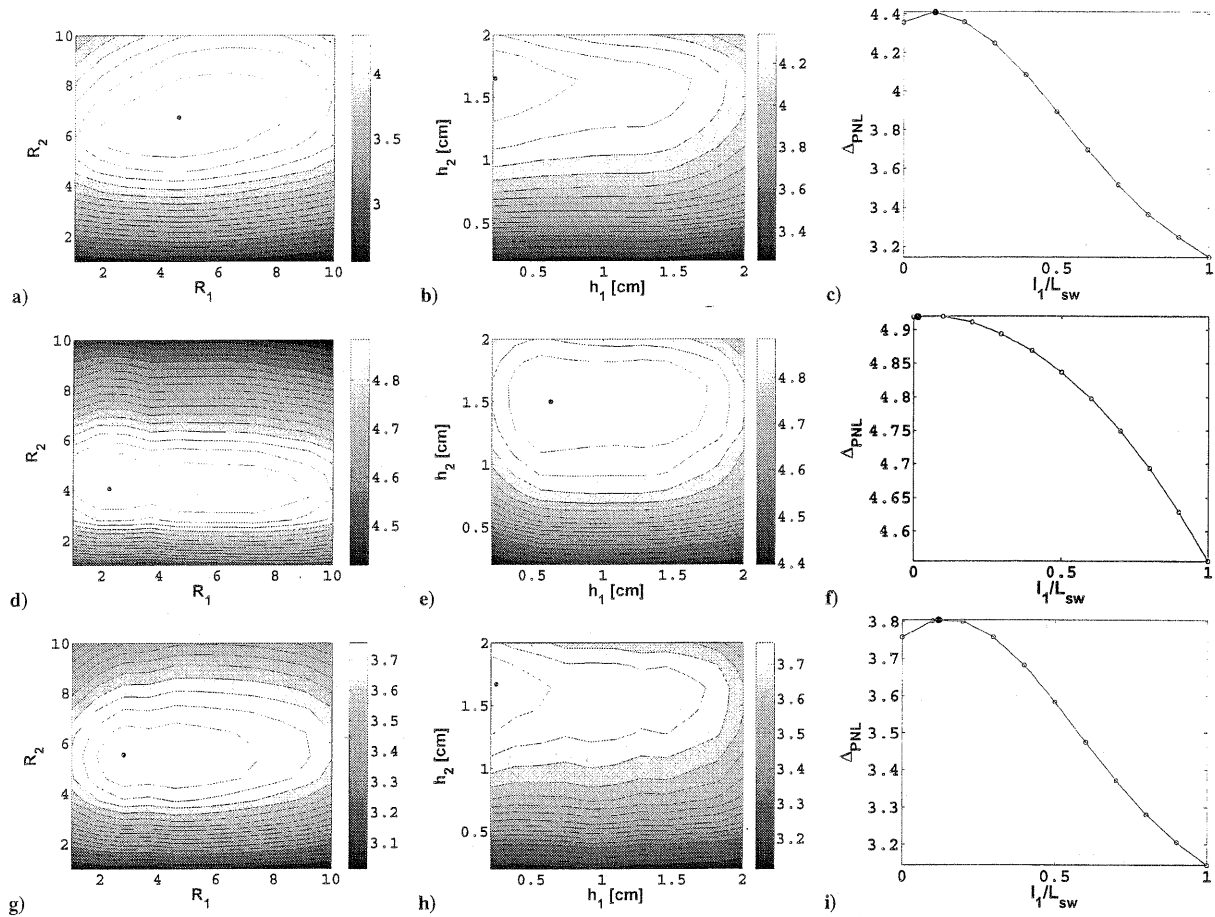
Fig. 9 Axially segmented liner, SM + MM model, Δ_{PNL} variation with respect to different combinations of R_1 and R_2 a, d, g, and j), h_1 and h_2 b, e, h, and k), and l_1/L_{sw} c, f, i, and l), at fan speeds a–c) sideline, d–f) cutback, g–i) approach, and j–l) AFS. Other variables fixed at optimum condition.

Table 8   Axially segmented liner, optimum liner parameters for AFS

Noise source	R_1	R_2	h_1, cm	h_2, cm	$l_1/L_{sw}\%$	AFS
		$R_1 \leq 10$ and $R_2 \leq 10$				
MM	2.2	4.5	0.58	1.52	3	1.61
SM	4.4	5.7	0.21	1.63	18	8.85
SM + MM	2.8	5.5	0.24	1.67	12	4.00
		$R_1 \leq 4$ and $R_2 \leq 4$				
SM	4	4	0.20	1.55	20	8.66
SM + MM	2.8	4	0.24	1.70	20	3.75

Table 9   Predicted Δ_{PNL} for each fan speed using optimum liner condition found for AFS problem used and $R \leq 10$

Noise source	Sideline	Cutback	Approach
MM	1.8	1.6	1.4
SM	6.7	13.8	——
SM + MM	4.46	4.8	1.26

Table 7 also lists the optimum found when the resistance is constrained to be $R \leq 4$. As before, at sideline, the MM source model converges to the same optimum configuration as the uniform liner. However, when the attenuation for the SM and SM + MM models at sideline is compared to the equivalent uniform liner cases, a gain in attenuation of 1.0 and 0.5 dB, respectively, is predicted.

Finally, Table 8 shows the attenuation predicted for a more realistic resistance range, $R \leq 4$, when the three source models are considered for the AFS problem. In Table 8 it is seen that, when $R \leq 4$, the predicted attenuation for the SM model is slightly less than when $R \leq 10$. When these values are compared to the uniform

liner optimum values in Table 6, it is seen that a significant increase in attenuation is predicted with an axially segmented liner. This means that the use of an axially segmented liner for tonal attenuation is effective, whereas for the combined noise source model (SM + MM) the combined effect of MM and SM sources yields less improvement in Δ_{PNL} reduction.

V.   Conclusions

In this paper, a systematic procedure that can be used to optimize inlet liners has been presented. The models and techniques proposed are robust and have been tested on two simple liner configurations, to produce a series of feasible and reproducible optimum values. An important intermediate result has been to demonstrate that the uncorrelated mode assumption that is utilized for the MM model is appropriate.

The main feature that emerges from the current study is that it is possible to increase the attenuation with an axially segmented liner only when a limited number of propagating modes are present. In fact, the MM source is not affected by the axial variation in the impedance. The high number of propagating modes cancels the potential benefit of the scattering at each impedance discontinuity.

When the SM model is used, an effective increase in attenuation of about 0.5 dB in PNL is predicted at AFS, with the optimum axially segmented liner compared with the optimum uniform liner. For the SM model, also note that for the highest fan speed an unrealistic value of the resistance is predicted. The optimum achieved for the SM model, with the resistance constrained to be less than four, is predicted to reduce the PNL by an additional 0.9 dB with the axially segmented liner compared with the uniform liner.

However, when the optimum results for the two noise sources combined (SM + MM) or for AFS are examined, the increase in

attenuation predicted with the axially segmented liner compared to the uniform liner is small.

Also, what emerges from this study is the presence of different optimum locations in the design space when more than two parameters are used. Even so, the optimizer is able to locate an absolute optimum in the design space. The presence of multiple optimal solutions, with similar attenuation, is not necessarily a disadvantage because it may be regarded as a kind of real-world flexibility in the decision process.

The aim of this study has been to demonstrate that an acoustic liner optimization is possible within acceptable processing time, using a mode-matching propagation model. The optimization takes into account tonal and broadband noise sources, over a broad range of frequencies, from 150 to 7500 Hz. Further work is planned, in which more complex liner impedance changes will be considered. This will also include the use of a realistic three-dimensional duct geometry and nonuniform mean flow profiles. This will require the use of numerical rather than analytic modeling techniques.

Appendix: Uncorrelated Modes

When an MM model is proposed, the main assumptions made are that the propagating modes are uncorrelated, so that each mode can be treated independently and that each mode carries an equal acoustic power. This assumption is commonly used[13] and is examined computationally here. Two papers by Zlavog and Eversman[45,46] on this topic have examined the influence of the phasing on broadband noise source specification. Specifically, in Ref. 46, a modal representation similar to the one proposed here is assumed. Then for a set of frequencies (the highest being $f = 2000$ Hz), four different random incident modal power phase distributions are assumed, showing that both source power and transmitted power tend to be normally distributed.

In this Appendix a wider frequency spectrum is examined. The main aim is to justify the use of the assumption that the modes are uncorrelated when modeling broadband noise by an MM source distribution. This is examined by showing how the transmission loss across the duct is affected by an MM source, in which the modes are taken to be coherent. In this paper, the optimization is based on an objective function that uses an approximate PNL evaluation. Therefore, the PNL is used as a test function when phase correlations are assigned. Usually, if the uncorrelated mode assumption is used, for a given frequency f, for each azimuthal mode m, the transmission of the propagating radial modes n are evaluated separately. Then, because the modes are assumed incoherent, the transmission loss can be found by simply summing the power in all of the propagating scattered modes. To determine how correlations between different modes can influence the solution (at a given frequency), a set of random phases is assigned to all of the propagating radial mode orders for a fixed azimuthal mode order. Therefore, for each of

the propagating azimuthal mode orders m, at the different frequencies considered, all of the cuton radial mode orders are specified at the source plane together, instead of each mode being propagated individually. Here the phases are assigned by using a pseudorandom number generator, being careful to not reproduce the same sequences of phases distributions in different realizations.

The MM source model uses the first 18 third-octave center frequencies to build the sound power transmission loss spectrum needed to evaluate the PNL. To generate a random sample of points as a base for our statistical study, 600 independent replications of the test are performed. The MM model was run for a fixed configuration, that is, fan speed and Mach number typical of a sideline flight condition, uniform liner resistance $R = 3$, and cavity depth $h = 1$ cm.

The sound power transmission loss distributions at the 18 third-octave center band frequencies are examined (Fig. A1) before comparing the predicted values of the PNL that are found with a random phase distribution, against the value predicted using the assumption that the modes are uncorrelated. Figure A1 shows how the sound power transmission loss Δ_{PWL} is influenced by phase variations. For the first six frequencies considered (Fig. A1, top row, $f = 150, 180, 240, 300, 375$, and 480 Hz) the sound power loss has a harmonic distribution. It reproduces the same distribution as a sine or cosine function for random values in the interval $[0, 2\pi]$. This is due to the small number of propagating modes at these frequencies. Then, as the number of propagating modes increases, $f \geq 600$ Hz, the Δ_{PWL} distribution tends to be Gaussian. Now, when the mean value Δ_{PWL} is used at each frequency, Fig. A2 shows the mean Δ_{PWL} spectrum for random phases, against the uncorrelated Δ_{PWL} spectrum. The main differences arise around the frequencies where
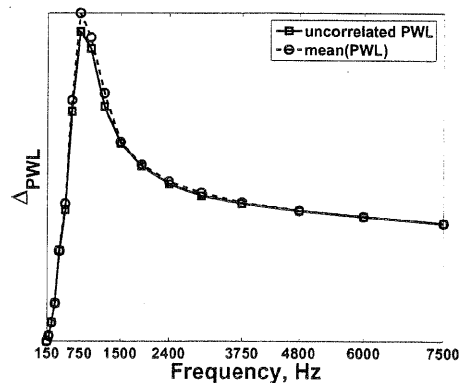

Fig. A2 Sound power transmission loss mean values spectrum against the uncorrelated Δ_{PWL} spectrum.
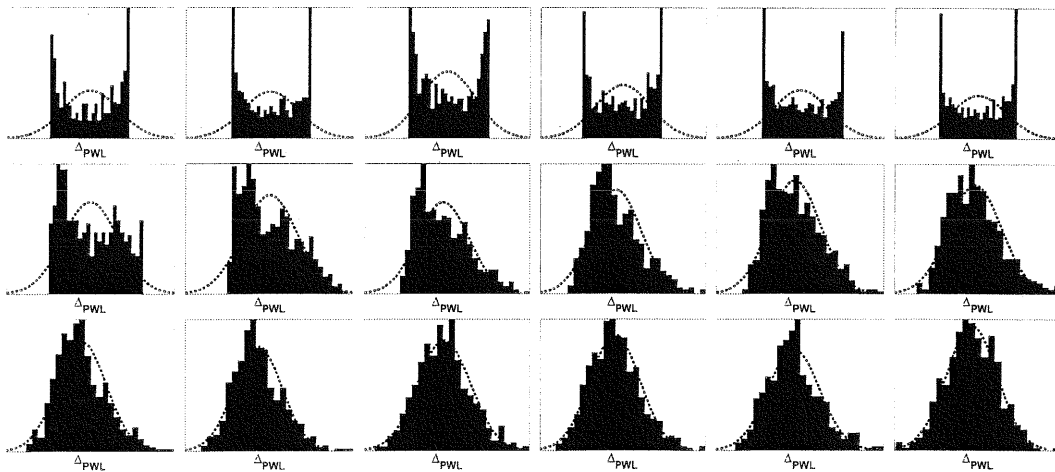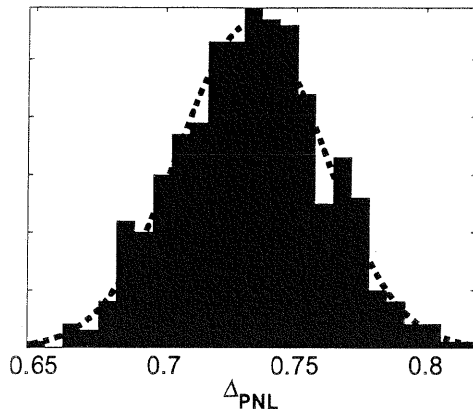

Fig. A1 Sound power transmission loss distribution at first 18 center third-octave-band frequencies, for random phase distribution among propagating modes.

Table A1   Predicted values of Δ_{PNL} for MM model

Uncorrelated	Random phase	
Δ_{PNL}	Mean (Δ_{PNL})	σ^a
0.728	0.733	0.028

[a] Observed Δ_{PNL} standard deviation when a random phase is assigned.

Fig. A3   PNL distribution due to random phase correlation.

the maximum attenuation is achieved. These are also the frequencies where the statistical behavior of the Δ_{PWL} distributions show a transition from harmonic to Gaussian.

Next, Fig. A3 shows the Δ_{PNL} distribution based on the different random phase distributions used. Finally, Table A1 lists the Δ_{PNL} values when the modes are assumed uncorrelated, as well as those when correlated with a random phase distribution.

From these data (and also as already shown) it is clear that the variation in Δ_{PNL} values arising from the differences between the uncorrelated and correlated models is small. The narrow bell variation of the Δ_{PNL} value along with the small standard deviation value of $\sigma = 0.0280$ demonstrates the limited degree of influence that a prescribed phase relation has in this example. This leads to the conclusion that an assumption of uncorrelated modes will have little effect on calculations of the sort reported here.

Acknowledgment

References

[1]Tyler, J. M., and Sofrin, T. G., "Axial Flow Compressor Noise Studies," *Transactions of the Society of Automotive Engineers*, Vol. 70, 1962, pp. 309–332.

[2]Mani, R., "Noise due to the Interaction of Inlet Turbulence with Isolated Stators and Rotors," *Journal of Sound and Vibration*, Vol. 17, No. 2, 1971, pp. 251–260.

[3]Mani, R., "Noise Generation by the Interaction Between Ingested Turbulence and a Rotating Fan," *Journal of Fluid Mechanics*, Vol. 359, 1998, pp. 181–216.

[4]Glegg, S. A. L., and Jochault, C., "Broadband Self-Noise from a Ducted Fan," *AIAA Journal*, Vol. 36, No. 8, 1998, pp. 1387–1395.

[5]Fisher, M. J., and Self, R. H., "Aeroacoustics Research in Europe: The CEAS-ASC Report on 2001 Highlights," *Journal of Sound and Vibration*, Vol. 258, No. 1, 2002, pp. 1–30.

[6]McAlpine, A., and Fisher, M. J., "On the Prediction of 'Buzz-Saw' Noise in Aero-engine Inlet Ducts," *Journal of Sound and Vibration*, Vol. 241, No. 1, 2001, No. 1, pp. 123–149.

[7]Gliebe, P., Mani, R., Shin, H., Mitchell, B., Ashford, G., Salamah, S., and Connell, S., "Aeroacoustic Prediction Codes," NASA Technical Rept. CR-2000-210244, Aug. 2000.

[8]Bailly, C., and Juvé, D., "Numerical Solution of Acoustic Propagation Problems Using Linearized Euler Equations," *AIAA Journal*, Vol. 38, No. 1, 2000, pp. 22–29.

[9]Atkins, H. L., "Continued Development of the Discontinuous Galerkin Method for Computational Aeroacoustic Applications," AIAA Paper 1997-1581, May 1997.

[10]Fang, Q. H., Hussaini, M. Y., and Rasetarineray, P., "An Analysis of the Discontinuous Galerkin Method for Wave Propagation Problems," *Journal of Computational Physics*, Vol. 151, 1999, pp. 921–946.

[11]Caruthers, J. E., French, J. C., and Raviprakash, G. K., "Greens Function Discretization for Numerical Solution of the Helmholtz Equation," *Journal of Sound and Vibration*, Vol. 187, No. 4, 1995, pp. 553–568.

[12]Eversman, W., "Theoretical Models for Duct Acoustic Propagation and Radiation," *Aeroacoustics of Flight Vehicles: Theory and Practice*, edited by H. H. Hubbard, Vol. 2, 1991, pp. 101–163.

[13]Bielak, G. W., Premo, J. W., and Hersh, A. S., "Advanced Turbofan Duct Liner Concepts," NASA Technical Rept. CR-1999-209002, Feb. 1999.

[14]Rice, E. J., "Optimum Wall Impedance for Spinning Modes—A Correlation with Mode Cutoff," *Journal of Aircraft*, Vol. 16, No. 5, 1979, pp. 336–343.

[15]Rice, E. J., "Modal Propagation Angles in Ducts with Soft Walls and Their Connection with Suppressor Performace," *Journal of Aircraft*, Vol. 16, No. 5, 1979, pp. 336–343.

[16]Rice, E. J., "Acoustic Liner Optimum Impedance for Spinning Modes with Mode Cutoff Ratio as Design Criterion," AIAA Paper 76-516, May 1979.

[17]Tsai, M. S., "Mode Scatter Design for Fan Noise Suppresion in Two-Dimensional Ducts," *Journal of Sound and Vibration*, Vol. 83, No. 4, 1982, pp. 501–512.

[18]Hamilton, J. A., and Astley, R. J., "Mid Frequency Theoretical Optimisation of an Intake Lip Liner for T700 Static Tests," Silencer Consortium, Technical Rept. D1.2-3.4-17, Southampton, England, U.K., Nov. 2002.

[19]Lafronza, L., McAlpine, A., Keane, A. J., and Astley, R. J., "Computer Aided Liner Optimization for Broadband Noise," AIAA Paper 2004-3029, May 2004.

[20]Fuller, C. R., "Propagation and Radiation of Sound from Flanget Circular Ducts with Circumferentially Varying Wall Admittances, I: Semi-infinite Ducts," *Journal of Sound and Vibration*, Vol. 93, No. 3, 1984, pp. 321–340.

[21]Fuller, C. R., "Propagation and Radiation of Sound from Flanget Circular Ducts with Circumferentially Varying Wall Admittances, II: Finite Ducts with Sources," *Journal of Sound and Vibration*, Vol. 93, No. 3, 1984, pp. 341–351.

[22]Watson, W. R., "An Acoustic Evaluation of Circumferentially Segmented Duct Liners," *AIAA Journal*, Vol. 22, No. 9, 1984, pp. 1229–1234.

[23]Campos, L., and Oliveira, J., "Optimization of Circumferentially Nonuniform Acoustic Liners in Annular Ducts," AIAA Paper 2004-3034, May 2004.

[24]Cummings, A., "High Frequency Ray Acoustics Models for Duct Silencers," *Journal of Sound and Vibration*, Vol. 221, No. 4, 1999, pp. 681–708.

[25]Lansing, D. L., and Zorumski, W. E., "Effects of Wall Admittance Changes on Duct Transmission and Radiation of Sound," *Journal of Sound and Vibration*, Vol. 27, No. 1, 1973, pp. 85–100.

[26]"Noise Standard: Aircraft Type and Airworthiness Certification," Advisory Circular AC36-4C, U.S. Dept. of Transportation, Federal Aviation, Administration, July 2003.

[27]Jones, R. H., and Montgomery, D. C., *Response Surface Methodology: Process and Product Optimization Using Design of Experiments*, Wiley, New York, 1995.

[28]Sacks, J., Welch, W., Mitchell, T. J., and Wynn, H. P., "Design and Analysis of Computer Experiments," *Statistical Science*, Vol. 4, No. 4, 1989, pp. 409–435.

[29]Jones, D. R., "A Taxonomy of Global Optimization Methods Based on Response Surfaces," *Journal of Global Optimization*, Vol. 21, No. 4, 2001, pp. 345–383.

[30]Keane, A. J., "The Options Design Exploration System, Reference Manual and User Guide," Ver. b3.1, URL: http://www.soton.ac.uk/~ajk/options.ps, March 2002.

[31]Abramowitz, M., and Stegun, I. A., *Handbook of Mathematical Functions*, NBS Applied Math Series 55 U.S. Dept. of Commerce, Washington, DC, Dec. 1955.

[32]Eversman, W., "Computation of Axial and Transverse Wave Numbers for Uniform Two-Dimensional Ducts with Flow Using a Numerical Integration Scheme," *Journal of the Acoustic Society of America*, Vol. 41, No. 2, 1975, pp. 252–255.

[33]Eversman, W., "Initial Values for the Integration Scheme to Compute the Eigenvalues for Propagation in Ducts," *Journal of the Acoustic Society of America*, Vol. 50, No. 1, 1977, pp. 159–162.

[34]Morfey, C. L., "Sound Transmission and Generation in Ducts with Flow," *Journal of the Acoustic Society of America*, Vol. 14, No. 1, 1971, pp. 37–55.

[35]Motsinger, R. E., and Kraft, R. E., "Design Performance of Duct Acoustic Treatment," *Aeroacoustics of Flight Vehicles: Theory and Practice*, edited by H. H. Hubbard, Vol. 2, No. 4, 1991, pp. 681–708.

[36]Rienstra, S. W., "A Classification of Duct Modes Based on Surface Waves," *Wave Motion*, Vol. 1107, No. 2, 2002, pp. 1–17.

[37]McAlpine, A., Astley, R. J., Hii, V. J. T., Baker, N. J., and Kempton, A. J., "Acoustic Scattering by an Axially-Segmented Turbofan Inlet Duct Liner at Supersonic Fan Speeds," *Journal of Sound and Vibration* (to be published).

[38]Jones, D. R., Schlonlau, M., and Welch, W. J., "Efficient Global Optimization of Expensive Black-Box Functions," *Journal of Global Optimization*, Vol. 13, No. 4, 1998, pp. 445–492.

[39]Lafronza, L., Song, W., McAlpine, A., Astley, R. J., and Keane, A. J., "Liner Optimization Using a Hybrid Finite Element Method," *Proceeding of 6th European Turbomachinery Conference*, edited by G. Bois, C. Sierverding, M. Marra, and T. Ars, Vol. 2, Lille, France, 2005, pp. 1085–1095.

[40]Keane, A. J., "Wing Optimization Using Design of Experiment, Response Surface and Data Fusion Methods," *Journal of Aircraft*, Vol. 40, No. 4, 2003, pp. 741–750.

[41]Song, W., and Keane, A. J., "A New Hybrid Updating Scheme for an Evolutionary Search Strategy Using Genetic Algorithms and Kriging," AIAA Paper 2005-1901, April 2005.

[42]Sobol, I. M., "On the Systematic Search in a Hypercube," *SIAM Journal on Numerical Analysis*, Vol. 16, No. 5, 1979, pp. 790–793.

[43]Goldberg, D. E., *Genetic Algorithms in Search, Optimization and Machine Learning*, Addison Wesley Longman, Reading, MA, 1989.

[44]Yuret, D., and de la Maza, M., "Dynamic Hill Climbing: Overcoming the Limitations of Optimization Techniques," *The Second Turkish Symposium on Artificial Intelligence and Neural Networks*, Istanbul, Turkey, 1993, pp. 254–260.

[45]Zlavog, G., and Eversman, W., "Source Effects on Relized Attenuation in Lined Ducts," AIAA Paper 2003-3247, May 2003.

[46]Zlavog, G., and Eversman, W., "A Statistically Based Computational Approach for Tonal and Broadband Noise Attenuation," AIAA Paper 2005-2900, May 2005.